Faraday Discussions

Cite this: *Faraday Discuss.*, 2014, **174**, 399

PAPER

Characterization and simulation of electrolyte-gated organic field-effect transistors

Katharina Melzer,* Marcel Brändlein, Bogdan Popescu, Dan Popescu, Paolo Lugli and Giuseppe Scarpa

Received 5th May 2014, Accepted 16th May 2014
DOI: 10.1039/c4fd00095a

In this work we fabricate and characterize field-effect transistors based on the solution-processable semiconducting polymer poly(3-hexylthiophene) (P3HT). Applying two independent gate potentials to the electrolyte-gated organic field-effect transistor (EGOFET), by using a conventional SiO_2 layer as the back-gate dielectric and the electrolyte-gate as the top-gate, allows the measurement of the electrical double layer (EDL) capacitance at the semiconductor–electrolyte interface. We record the transfer curves of the transistor in salt solutions of different concentration by sweeping the bottom gate potential for various constant electrolyte-gate potentials. A change of the electrolyte-gate potential towards more negative voltages shifts the threshold voltage of the bottom-gate channel towards more positive back-gate potentials, which is directly proportional to the capacitive coupling factor. By operating the EGOFET in the dual-gate mode, we can prove the dependency of the EDL capacitance on the molarity of the electrolyte according to the Debye–Hückel theory, and additionally show the difference between a polarizable and non-polarizable electrolyte-gate electrode. With the experimentally obtained values for the EDL capacitance at the semiconductor–electrolyte interface we can model the electrolyte-gate transfer characteristics of the P3HT OTFT.

1 Introduction

Organic thin-film transistors (OTFTs) have been explored for various sensing applications in recent years due to their easy and low-cost fabrication (for recent reviews refer to[1–3] and references therein). In particular, the semiconducting polymer poly(3-hexylthiophene) (P3HT) is well-established as the active semiconducting component in OTFTs for biosensing applications[4–9] due to several key features offered by the material: its outstanding biocompatibility,[10] its solution

Institute for Nanoelectronics, TU München, Arcisstrasse 21, 80333 München, Germany. E-mail: katharina.melzer@nano.ei.tum.de

processability and subsequent applicability in large-scale, flexible and cost-effective electronics, and its relatively high mobility.[11,12]

In organic thin-film transistors, in general a thin film of an organic semiconducting material is utilized as the active layer. Two contacts, the source and drain electrodes, which are in direct contact with the semiconducting material, are used to apply the source–drain voltage and to measure the current flowing between them through the organic semiconducting channel. As the third electrode, the gate electrode is used to control the number of charge carriers, in p-type material holes, in the semiconducting channel at the interface between the semiconductor and the gate dielectric through an electric field applied across the insulating gate dielectric. Therefore one can modulate the source–drain current flowing between the source and drain contacts by applying a given potential to the gate electrode. For a p-type material the transistor is turned "ON" for negative gate voltages, whereas a positive gate bias switches the device "OFF".[13]

In recent years the usage of solid and liquid electrolytes as gate dielectrics in OTFTs has gained great interest. They display a huge capacitance (C_G) compared to the conventional silicon dioxide (SiO_2), which is typically in the range of 1–100 μF cm^{-2}, ~1000 times higher than the one offered by a nm-thick SiO_2-layer.[1,12,14,15] Especially important in EGOFETs is the formation of an electrical double layer (EDL) at the electrolyte–semiconductor interface as well as the gate electrode–electrolyte interface. At the gate electrode–electrolyte interface the electronic charges close to the electrode surface are compensated by oppositely charged ions in the electrolyte close to the interface. At the electrolyte–semiconductor interface the EDL consists of ions forming the inner Helmholtz plane in the electrolyte and charge carriers in the semiconducting channel. Additionally, at both interfaces, hydrated ions of both charges accumulate and form the outer Helmholtz plane. In the bulk of the electrolyte, the potential stays constant as the diffuse layer of the hydrated positive and negative ions ensures charge neutrality.[12,15,16] The charge distribution in an EDL can be described by the Gouy–Chapman–Stern model.[17–20] In the case of a flat electrode surface, the electrostatic capacitance of the EDL can be related to the Debye length λ_D, which defines the distance d between the interface and the outermost layer of ions which is necessary to compensate the gate surface charge fully. The Debye length is inversely proportional to the square root of the ionic strength, according to:

$$C_{DL} \sim \frac{1}{\lambda_D} \tag{1}$$

$$\lambda_D = \sqrt{\frac{\varepsilon_r \varepsilon_0 k_B T}{2 C_0 N_A e^2}} \tag{2}$$

where C_{DL} represents the capacitance of the electrical double layer, λ_D is the Debye length, the parameters ε_r and ε_0 are the relative and the vacuum permittivity, respectively, k_B is the Boltzmann constant, T is the temperature, C_0 is the ionic strength of the electrolyte, N_A is the Avogadro constant and e is the elementary charge.[19] Since the thickness of the electrical double layer is on the sub-nm length scale (a few Å to nm), the capacitance per unit area is typically in the range of tens of μF cm^{-2}. This huge gate capacitance allows a transistor to operate at very low voltages: already gate potentials of around 0.5 V are sufficient

to accumulate enough charge carriers in the semiconducting channel to turn the device "ON". By exploiting the electrical double layer capacitance one can modulate the transistor current response extremely effectively. Another very important advantage of electrolyte-gated organic thin-film transistors is the convenient integration into biosensors operated in liquid environments. One is in fact independent from the choice of the substrate,[21,22] and the analyte is already in direct contact with the active semiconducting layer. Since the accumulation of charge carriers in the semiconducting channel and therefore also the source–drain current can be altered by the adsorption of charged analytes on the semiconductor surface or a change in the amount of solute ions in the electrolyte, electrical detection of certain species is possible.

Therefore it is of great interest for various sensing applications with EGOFETs to obtain information about how changes to the electrolyte–semiconductor interface, especially to the electrical double layer and its capacitance, influence the transistor characteristics.

In this work we concentrate on the influence of the electrical double-layer capacitance (C_{DL}) and try to gain information about the dependency of C_{DL} on the ionic strength of the electrolyte. We operate the OTFT based on the semiconducting polymer poly(3-hexylthiophene) (P3HT) in the so-called dual-gate mode[23] by using both a conventional back-gate as well as an electrolyte-gate as the top-gate. Exploiting the capacitive coupling factor[23,24] allows us to extract the double-layer capacitance from several back-gate sweeps with different constant electrolyte-gate potentials. Changing the ionic strength of the aqueous potassium chloride (KCl) solution used as the gate dielectric for the electrolyte-gate gives us the double-layer capacitance as a function of the salt concentration. We demonstrate that the capacitance of the electrical double layer at the semiconductor–electrolyte interface increases with an exponential increase of the ionic strength of the electrolyte. In addition to the electrical characterization of the organic thin-film transistors, we compare the results to theoretical data gained from simulations with a modified drift–diffusion model.

2 Experimental

2.1 Device fabrication

Organic thin-film transistors (OTFTs) were processed using highly p-doped silicon wafers (Si-Mat) as a substrate with a thermally grown 65 nm thick silicon dioxide layer (SiO_2) as the conventional gate dielectric. Source and drain electrodes (5 nm Cr as adhesion layer, 40 nm Au) were patterned on top of the oxide layer by a conventional negative optical photolithography process. An interdigitated finger structure (IDES) was used as the electrode structure, with a channel length of 50 μm and a width-to-length ratio of 900. A 1 wt% solution of regioregular poly(3-hexylthiophene) (P3HT, Rieke Metals) in anhydrous 1,2-dichlorobenzene (DCB, VWR) was prepared and stirred for 30 min to obtain a homogeneous solution. The solution was then filtered through a polytetrafluoroethylene (PTFE) syringe filter with a pore size of 200 nm (VWR) and spin-coated (1000 rpm, 90 s) onto the surface of the wafer in a glove box system (N_2). After spin-coating, the film was annealed on a hot plate under a nitrogen atmosphere at 150 °C for 20 min. The obtained polymer layer was approximately 50 to 70 nm thick. Atomic force microscopy (AFM, Jeol, JSPM-5200) measurements

yielded an R_q value of 3.4 nm, which is a measure for the surface roughness of the polymeric film, and a peak-to-valley distance of about 22 nm.

2.2 Electrical characterization

Transfer characteristics (I_D *vs.* V_G) and output characteristics (I_D *vs.* V_{DS}) of the devices were recorded using a Keithley 4200-SCS semiconductor parameter analyser system. To operate the transistor in liquid, measurements were performed after mounting the devices in a PDMS flow-chamber, which has a liquid compartment volume of 100 μL. The transfer characteristics of the OTFT were obtained by sweeping either the back-gate potential ($V_{DS} = -10$ V) or the electrolyte-gate potential ($V_{DS} = -0.1$ V), while a constant drain voltage V_{DS} was applied. For the back-gate sweep no electrolyte was on top of the semiconducting layer, whereas for the electrolyte-gate sweep the back-gate electrode was left floating. The electrolyte-gate potential was chosen from the relatively small voltage regime between $V_{TgS} = +0.6$ V and $V_{TgS} = -0.6$ V to avoid any water hydrolysis or any other electrochemical reaction at the gate electrode or the semiconductor surface.[12]

For the measurement of the electrical double layer capacitance, the potential at the electrolyte-gate electrode, either a Pt wire or a homemade Ag/AgCl electrode, was kept constant while a scan of the back-gate voltage between $V_{BgS} = +20$ V and $V_{BgS} = -7.5$ V was performed. The back-gate sweep was recorded for six different electrolyte-gate potentials between $V_{TgS} = +0.1$ V and $V_{TgS} = -0.4$ V, whereas the drain voltage was kept constant for each back-gate sweep at $V_{DS} = -0.1$ V. All characterization measurements were performed in ambient conditions. The electrolyte was exchanged manually using a Gilson pipette. After exchanging the electrolyte the system was left to equilibrate for 5 minutes before the next measurement was started.

2.3 Preparation of electrolytes

The electrical double layer capacitance was characterized using either deionized water (DI-H_2O, classified with a resistivity of 18.2 MΩ cm). Potassium chloride solutions were prepared by dissolving 100 mM KCl (≥99.0%, Sigma Aldrich) in DI-H_2O and further diluting it with DI-H_2O to the desired KCl concentrations.

3 Results and discussion

3.1 Device characteristics

The transfer characteristics of the OTFT were obtained by sweeping either the back-gate potential or the electrolyte-gate potential, while a constant drain voltage V_{DS} was applied. For the back-gate sweep no electrolyte was on top of the semiconducting layer, whereas for the electrolyte-gate sweep the back-gate electrode was left floating. Fig. 1(a) shows the source–drain current I_D *versus* the back-gate potential; the drain voltage was kept constant at $V_{DS} = -10$ V. Fig. 1(b) shows I_D *versus* the electrolyte-gate potential V_{TgS} of the OTFT gated with a Pt electrode in a 10 mM solution of KCl in DI-water as the electrolyte; the drain voltage was kept constant at $V_{DS} = -0.1$ V. Both transfer curves exhibit typical p-type field-effect characteristics with ON/OFF ratios of around 100. When the OTFT is operated with the conventional silicon dioxide (SiO_2, 65 nm, $C_{Ox} = 53.2$ nF cm^{-2}) back-gate,

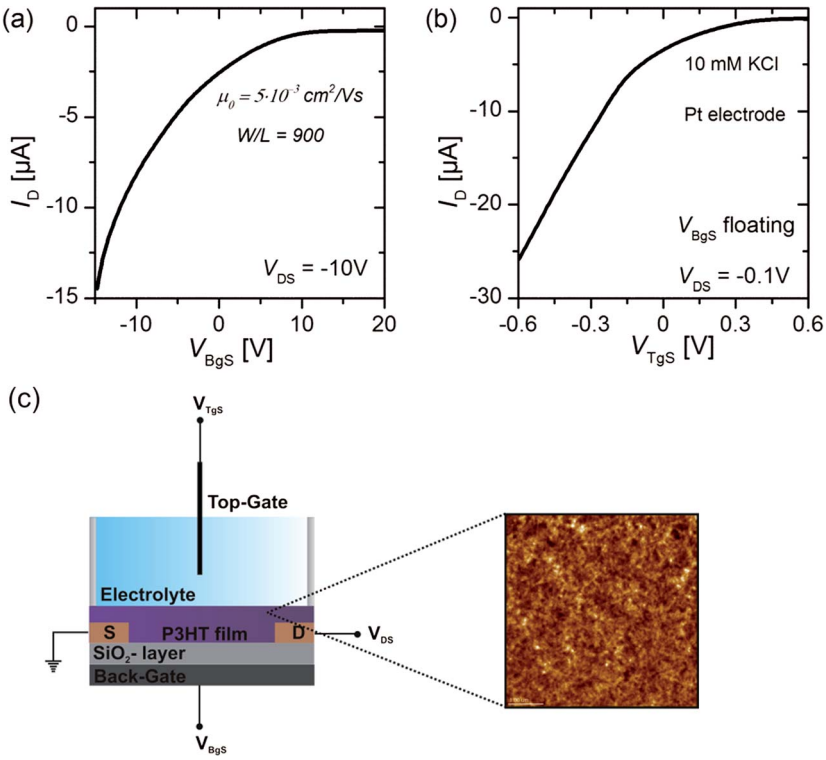

Fig. 1 (a) Transfer characteristics of a back-gated P3HT OTFT. (b) Transfer characteristics of an electrolyte-gated P3HT OTFT recorded in a 10 mM KCl solution. A Pt wire was used as the electrolyte-gate electrode. The back-gate electrode was left floating. (c) Schematic representation of a dual-gated P3HT OTFT. A 65 nm thick SiO_2-layer was used as the back-gate dielectric, whereas various electrolytes serve as the top-gate dielectric. The magnification shows an AFM scan (scan size 5 µm × 5 µm) of the spin-coated P3HT layer on a SiO_2 surface. The obtained polymer layer was approximately 50 to 70 nm thick. It yielded an R_q value of 3.4 nm and a peak-to-valley distance of about 22 nm.

the transfer curve reveals a transconductance of $g_m = 2.4$ µS. The transconductance of organic thin-film transistors is usually given by

$$g_m = \frac{W}{L}\mu_0 C_G V_{DS}, \quad (3)$$

where W and L are the channel width and length, respectively, μ_0 is the charge carrier mobility, C_G is the capacitance of the gate dielectric, and V_{DS} is the drain voltage.

The mobility calculated according to eqn (3) equals $\mu_0 = 5 \times 10^{-3}$ cm^2 V^{-1} s^{-1} and is comparable to the literature values obtained with OTFTs based on P3HT.[11,25] From Fig. 1(b) it is obvious that the electrolyte-gated OTFT delivers higher I_D currents at an electrolyte-gate voltage of $V_{TgS} = -0.6$ V and a drain bias of $V_{DS} = -0.1$ V, as compared to the SiO_2-gated device with V_{BgS} potentials in the range of 10 V, although the same width-to-length ratio ($W/L = 900$) was used. From a linear fit of the transfer curve we can extract a transconductance value of $g_m = 46.0$ µS. The higher the current, the higher the transconductance, and the

lower operating voltages reflect the greatly enlarged gate capacitance of the electrical double layer relative to the 65 nm thick SiO_2-layer. In order to derive the mobility from the transfer curves of the electrolyte-gated OTFT, we first have to measure the capacitance of the electrical double layer.

3.2 Measurement of the electrical double layer capacitance

To measure the capacitance of the electrical double layer, we operate the OTFT in the so-called dual-gate mode[23] by using both the conventional silicon dioxide (SiO_2, 65 nm) back-gate as well as an additional electrolyte-gate. The transfer curves (I_D *vs.* V_{BgS}) of the back-gated transistor can be shifted by applying various fixed voltages to the electrolyte-gate electrode immersed in an aqueous solution (see Fig. 1(c)). Here the potential at the electrolyte-gate electrode was kept constant, while a sweep of the back-gate voltage was performed between $V_{BgS} =$ +20 V and $V_{BgS} = -7.5$ V. If the applied electrolyte-gate voltage is negative, a semiconducting channel at the electrolyte–polymer interface is formed and the charge carrier accumulation in the semiconducting layer can be controlled by sweeping the back-gate voltage. A back-gate sweep was recorded for six different electrolyte-gate potentials between $V_{TgS} = 0.1$ V and $V_{TgS} = -0.4$ V. The resulting transfer curves with DI-water as the electrolyte and a Pt wire as the gate electrode are shown in Fig. 2(a). The obtained transfer curves first exhibit a short charging phase and then follow a linear dependence for I_D *vs.* V_{BgS}. According to a theoretical model for dual gate transistors,[24] the source–drain current of a dual-gated OTFT in the linear regime can be expressed as follows:[23]

$$I_D = \frac{W}{L}\mu_0\left(C_{DL}V_{TgS} + C_{Ox}V_{BgS} + \sigma_i\right)V_{DS}, \quad (4)$$

where W is the width and L is the length of the channel, μ_0 is the mobility, C_{Ox} is the capacitance of the SiO_2 layer, C_{DL} is the electrical double layer capacitance, and V_{DS}, V_{TgS} and V_{BgS} are the drain voltage, the electrolyte-gate potential and the back-gate potential, respectively. According to eqn (4), the threshold voltage of the back-gate sweep $V_{BG,th}$, which is defined as the back-gate voltage where the

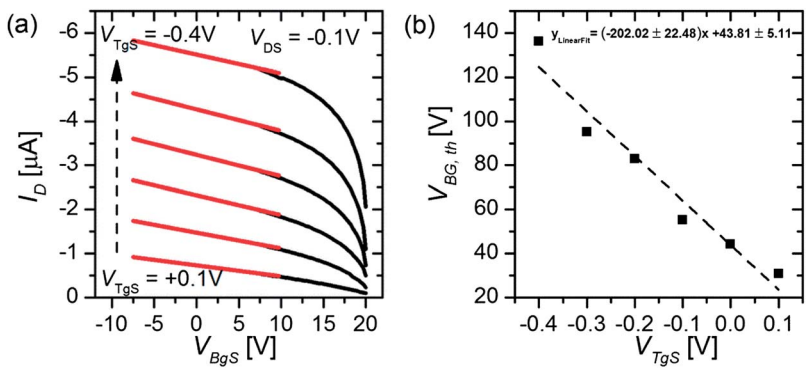

Fig. 2 (a) Back-gate transfer curves (black lines) at $V_{DS} = -0.1$ V recorded in DI-water with a Pt gate electrode and linear fits (red lines) at different electrolyte-gate voltages V_{TgS}. (b) Threshold voltages extracted from the linear fit curves of the back-gate sweeps as a function of the electrolyte-gate potential and the corresponding linear fit curve.

source–drain current equals zero, is directly proportional to the applied electrolyte-gate potential modulated by the capacitive coupling factor C_{DL}/C_{Ox}:[23]

$$V_{BG,th} \propto -\frac{C_{DL}}{C_{OX}} V_{TgS}. \quad (5)$$

The threshold voltages were extrapolated from a linear fit (red lines, Fig. 2(a)) of the various transfer curves and plotted as a function of the applied top-gate voltage V_{TgS}, as depicted in Fig. 2(b).

By using the slope k obtained from the linear fit of the $V_{BG,th}$ *vs.* V_{TgS} dependence and taking into account the capacitance of the back-gate dielectric (thickness $d_{Ox} = 65$ nm, $C_{Ox} = 53.2$ nF cm^{-2}), the capacitance of the electrical double layer can be calculated according to eqn (5) (ref. 23).

We obtain a double layer capacitance of C_{DL} (DI-H_2O) $= 10.8 \pm 1.2$ μF cm^{-2}, which exceeds the literature values for P3HT in contact with deionized water (3–6 μF cm^{-2}), as measured by impedance spectroscopy, by a factor of 2, but they are consistent with values obtained for metallic surfaces in contact with an electrolyte, ~20 μF cm^{-2} for gold in contact with DI-water.[12] Cramer *et al.*[23] determined the double layer capacitance with a pentacene thin-film transistor with deionized water as the electrolyte. They obtained values of C_{DL} (DI-H_2O) $= 7.8$ μF cm^{-2},[23] which is generally lower than the results obtained with the P3HT OTFT. One possible explanation could be that their semiconducting layer consists of less than six monolayers of pentacene and therefore has a much smoother surface than the P3HT film (see the AFM image in Fig. 1(c)) used in this work. In simplified terms, the huge surface roughness of the P3HT film results in an increased capacitance of the electrical double layer at the semiconductor–electrolyte interface since the geometrical size of the active area (4 mm × 4 mm) stays constant, whereas the effective contact area between the electrolyte and semiconductor increases with increasing surface roughness.

In general, the capacitance of the Debye–Helmholtz layer depends on the ionic strength of the electrolytic solution (see eqn (1) and (2)), therefore back-gate sweeps were not only recorded for different top-gate voltages but also in KCl solutions with varying ion concentrations. The obtained values for the double layer capacitance measured with a Pt wire as the gate electrode are shown in Fig. 3(a). The reduction of the capacitance to lower ionic strengths is in general agreement with theoretical models describing the Debye–Helmholtz layer.[17–19] Again, the value obtained by Cramer *et al.*[23] for a 100 mM solution of a monovalent salt (sodium chloride, NaCl) C_{DL} (100 mM NaCl) $= 14.6$ μF cm^{-2} is lower than the EDL capacitance measured with the P3HT OTFT.

Additionally, the same measurements were performed with an Ag/AgCl electrode. The main difference between these two gate materials is that platinum can be seen as an ideally polarizable electrode when operated in an electrolytic solution with these relatively low voltages ($|V_{TgS}| < 1$ V), which means that an electrical double layer forms at the interface between the gate-material and the electrolyte. However, due to the following reaction constantly taking place at the surface of the Ag/AgCl electrode, a steady-state current flows from the gate electrode to the electrolytic solution, and therefore no electrical double layer forms at the interface between the electrode and the electrolyte.[26]

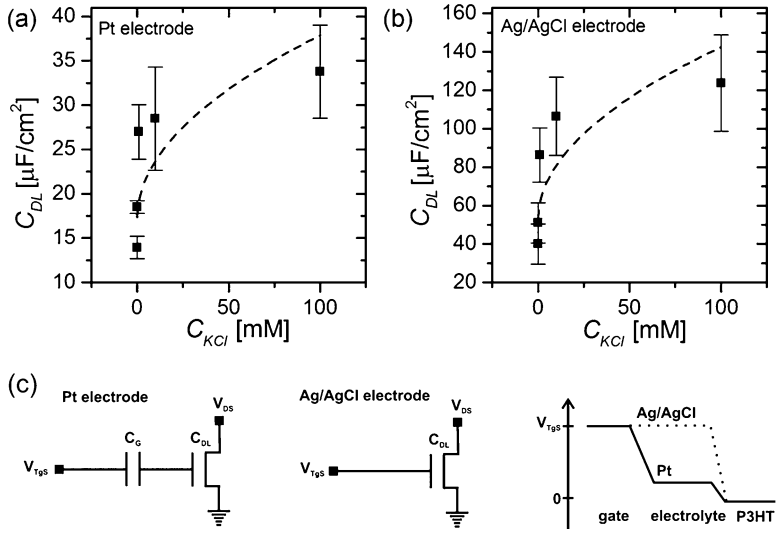

Fig. 3 Capacitance of the electrical double layer C_{DL} obtained (a) for a Pt-gated transistor and (b) with an Ag/AgCl electrode as the gate electrode as a function of the salt concentration. Panel (c) shows the equivalent circuits[28] of a Pt gate electrode and an Ag/AgCl electrode immersed in the electrolytic solution. The right graph depicts the potential distribution between the gate electrode and the semiconducting channel for both electrode types.[26]

$$Ag + Cl^- \leftrightarrow AgCl + e^- \tag{6}$$

This means that with a Pt wire immersed as the gate electrode in the electrolytic solution, the applied gate potential drops across two electrical double layers formed both at the electrode–electrolyte interface as well as at the electrolyte–semiconductor interface. On the contrary, for an Ag/AgCl electrode the whole potential has to drop across the electrical double layer formed at the electrolyte–semiconductor interface (see Fig. 3(c)).[19,20,27,28]

In a simple equivalent circuit, the Pt wire immersed in the electrolytic solution can be regarded as a capacitor C_G (see Fig. 3(c)), which is connected in series with the capacitor C_{DL} of the interface between the P3HT layer and the electrolytic solution, as shown in Fig. 3(a). Thus the effective gating capacitance of the OTFT operated with a Pt electrode is given by:[28]

$$C_{eff,Pt} = \frac{C_G C_{DL}}{C_G + C_{DL}}. \tag{7}$$

Therefore one would expect to measure a higher double layer capacitance C_{DL} by operating the device with an Ag/AgCl electrode. Fig. 3(b) shows the double layer capacitance measured with an Ag/AgCl electrode as a function of the salt concentration present in the electrolyte.

For a KCl concentration of 100 mM we obtain a double layer capacitance of C_{DL} (100 mM KCl, Ag/AgCl) = 123.77 ± 2.50 µF cm^{-2}, which is about 4 times higher than with a Pt electrode, where C_{DL} (100 mM KCl, Pt) = 33.78 ± 5.25 µF cm^{-2}.

3.3 Simulation of electrolyte-gated field-effect transistors

For the simulation of the back-gated and electrolyte-gated OTFT devices we use a modified drift–diffusion model implemented into the commercial TCAD software Sentaurus. For a given device geometry, this software simulates charge transport by solving a set of equations, including the drift–diffusion equations, the continuity equations and the Poisson equation

$$J_n = -e\mu_n\nabla\phi + eD_n\nabla n, \tag{8}$$

$$J_P = -e\mu_p\nabla\phi - eD_p\nabla p, \tag{9}$$

$$\nabla\cdot J_n = e(R - G), \tag{10}$$

$$\nabla\cdot J_p = -e(R - G), \tag{11}$$

$$\nabla\cdot(\varepsilon_0\varepsilon_r\nabla\phi) = e(n - p + N_D^+ - N_A^- + p_{At}), \tag{12}$$

where J_n (J_p) is the electron (hole) current density, n (p) is the electron (hole) density, μ_n (μ_p) is the electron (hole) mobility, D_n (D_p) is the electron (hole) diffusion coefficient, ϕ is the electrostatic potential, G and R are the net generation and recombination rates and p_{At} is the density of trapped holes. To account for the particularities of organic materials, three modifications are implemented.[29,30] Firstly, a low contact barrier height from the source to HOMO level of the semiconductor material ensures easy injection of holes, giving the device p-type conductivity. Secondly, a Poole–Frenkel-type field-dependent mobility needs to be considered:

$$\mu = \mu_0(T)\exp\left(\sqrt{E/E_0}\right), \tag{13}$$

where $\mu_0(T)$ is the low field mobility, E is the electric field and E_0 is an effective parameter of approximately 3×10^5 V cm^{-1}. Thirdly, an interface trap model at the oxide–P3HT interface and the electrolyte–semiconductor interface effectively models the hopping-assisted charge transport. Here, an exponential energy distribution of two different trap levels, a shallow trap at 0.1 eV and a deeper trap at 0.4 eV, from the HOMO level is considered. Such a broad energy distribution is justified by the use of standard spin-coating techniques for the deposition of the organic semiconductor, inevitably introducing defects into the P3HT active region.

In a first approximation, the electrolyte will be taken into account as an insulating layer between the electrolyte-gate contact and the organic semiconductor region, according to the simple Helmholtz model (see Fig. 4(a)).[31]

That way, the electrical double layer is modelled as a parallel plate capacitor (from here on referred to as the Helmholtz layer) accounting for a linear potential drop. The capacitance of this Helmholtz layer is taken from the experimentally extracted data to 28 μF cm^{-2} for an ion concentration of 10 mM, according to Section 3.2. As can be seen in Fig. 4(b), when operating with the top-gate contact the conductive channel is spatially shifted towards the electrolyte–semiconductor interface. This can be intuitively understood considering the electric field that is generated by the applied negative top-gate voltage and which attracts positive charge carriers towards this interface. The considerably low top-gate voltage is

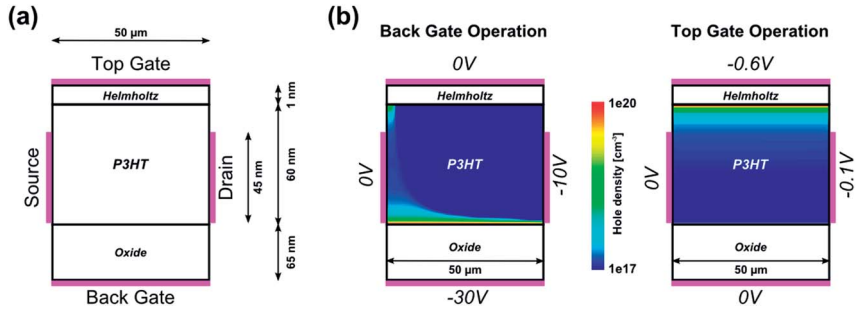

Fig. 4 (a) Drift–diffusion simulation layout for the Helmholtz model. The electrolyte is taken into account by an insulating Helmholtz layer. (b) Comparison of back-gate operation and top-gate operation. The values of the boundary conditions are given at the respective contacts and are typical for the different operation modes. The hole density gives information as to where the conducting channel is formed.

due to the large capacitive value of the Helmholtz layer compared to the oxide layer of the back-gate contact.

With this simulation setup, we simulate transfer and output curves in both back-gate and top-gate operation and compare them to experimental data to adjust the simulation parameters. The simulation of the back-gate operation has already been reported in the literature,[32] and serves as a reference for the simulation parameters of the organic semiconductor material, such as density of states, unintentional doping, trap level distribution, low field mobility *etc.* These parameters are then used for the simulation of top-gate operation to give a conclusive self-consistent picture. All relevant simulation parameters are given in Table 1. The results of such a fitting procedure are shown in Fig. 5 for one selected device. The simulation of transfer curves in back-gate operation (Fig. 5(a)) shows good agreement with the experimental data in the accessible voltage range, and also the output curve is in the right order of magnitude. The low field mobility in that case is $\mu_0 = 5 \times 10^{-3}$ cm^2 V^{-1} s^{-1}, which is in good agreement with literature values.[11,25] When simulating the top-gate operation (Fig. 5(b)), one can see that using this value for the low field mobility leads to a drastic underestimation of the drain current. There are two parameters in our model which affect the transconductance of the device, *i.e.* the slope of the linear transistor behaviour, the first being the capacitance of the Helmholtz layer and the second being the low field mobility. By changing the Helmholtz layer capacitance one would have to use unphysical values that are several orders of magnitude larger than what has been extracted experimentally, in order to fit the experimental data. Furthermore, this leads to large deviations from the experimental data in the sublinear regime as the curve becomes heavily kinked.

On the other hand, when changing the mobility by about one order of magnitude, the transconductance of the experimental data can be matched correctly and also the deviations in the sublinear regime are not as pronounced. Such an elevated low field mobility hints at a physical change in the transport properties at the electrolyte–semiconductor interface. Cramer *et al.*[33] stated that the reorientation of water dipoles at the electrolyte–semiconductor interface stabilizes positive charge carriers and leads to a polaronic trap state which

Table 1 Simulation parameters for back-gate and top-gate operation

		Device T#01
P3HT	LUMO	3 eV
	HOMO	5 eV
	ε_r	3
	DOS	5×10^{20} cm^{-3}
Doping concentration	N_D	1.2×10^{17} cm^{-3}
Poole–Frenkel mobility	μ_0 (back)	5×10^{-3} cm^2 V^{-1} s^{-1}
	μ_0 (top)	3×10^{-2} cm^2 V^{-1} s^{-1}
	E_0	3×10^5 V cm^{-1}
Shallow level trap	$c_{0,shall}$	5×10^{12} cm^{-2}
	E_{mid}	0.1 eV
	E_{sig}	0.2 eV
Deep level trap	$c_{0,deep}$	5×10^{12} cm^{-2}
	E_{mid}	0.4 eV
	E_{sig}	0.3 eV
Fixed charges	c_{fix} (back)	-2.1×10^{12} cm^{-2}
	c_{fix} (top)	-2.1×10^{12} cm^{-2}

remains highly mobile in the plane parallel to the interface. Their findings based on pentacene show a mobility elevated by about one order of magnitude.

They mention that the polaron binding energy depends only on water polarization and the spatial extension of the charge carriers in the organic semiconductor. Therefore, these findings can be generalized to other organic semiconductors and might give an explanation for the different mobilities for back-gate operation *versus* top-gate operation in our sensor devices. However, further investigations are needed in that direction.

In order to refine the simple approximation of the EDL as a parallel plate capacitor, one needs to account for a diffusive layer, the Gouy–Chapman layer, in

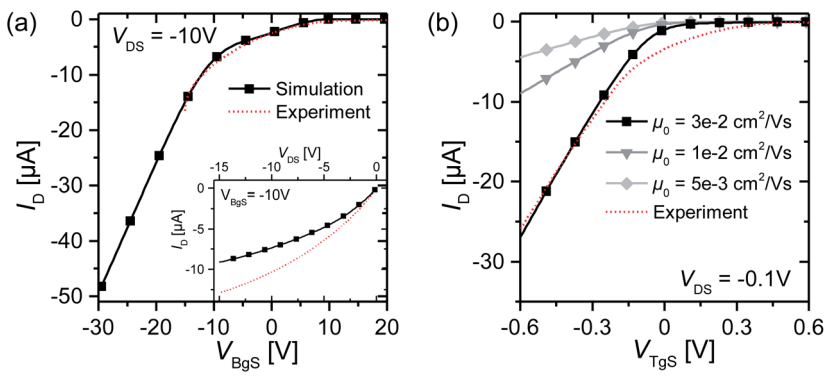

Fig. 5 (a) Best fit of the back-gate operation transfer curve for one selected device. The inset shows an output curve at $V_{BgS} = -10$ V. The mobility is $\mu_0 = 5 \times 10^{-3}$ cm^2 V^{-1} s^{-1}. (b) Fit of the top-gate operation transfer curve for device T#01 for different low field mobilities according to the Helmholtz model. The ion concentration in the electrolyte is 10 mM. All simulation parameters can be found in Table 1.

the form of the Poisson–Boltzmann equation (PBe) according to the Stern model.[34] The PBe reads

$$\nabla(\varepsilon_0\varepsilon_r\nabla\phi) = -\sum_{i=1}^{N} z_i e c_{i,0} \exp\left(-\frac{z_i e(\phi - V_{TgS})}{k_B T}\right), \quad (14)$$

where the sum goes over all ion species present in the electrolyte, z_i is the valency and $c_{i,0}$ the bulk concentration of ion species i. This is already under investigation and will be the topic of a future contribution.

4 Conclusion

In summary, we reported the measurement of the electrical double layer capacitance of a dual-gated P3HT OTFT by sweeping the back-gate potential with fixed electrolyte-gate potentials at the top-gate. We proved the dependency of the EDL capacitance on the ionic strength of the electrolyte and additionally we demonstrated the effect of a non-polarizable gate electrode in comparison to a polarizable electrode on the gating mechanism. With the experimentally obtained values for the capacitance of the Debye-Helmholtz layer at the semiconductor–electrolyte interface, we can model the electrolyte-gate transfer characteristics of the P3HT OTFT. Our study suggests that the mobility of the active material close to the semiconductor–electrolyte interface is larger than the bulk mobility.

Acknowledgements

This work was partially supported by the International Graduate School for Science and Engineering (IGSSE), the Graduate School (TUM-GS) at the Technische Universität München, and the European Integrated Training Networks "Olimpia" and "OrgBio".

References

1 L. Kergoat, B. Piro, M. Berggren, G. Horowitz and M.-C. Pham, *Anal. Bioanal. Chem.*, 2012, **402**, 1813–1826.
2 P. Lin and F. Yan, *Adv. Mater.*, 2012, **24**, 34–51.
3 J. T. Mabeck and G. G. Malliaras, *Anal. Bioanal. Chem.*, 2006, **384**, 343–353.
4 A. M. Münzer, K. Melzer, M. Heimgreiter and G. Scarpa, *Biochim. Biophys. Acta*, 2013, **1830**, 4353–4358.
5 C. Bartic, B. Palan, A. Campitelli and G. Borghs, *Sens. Actuators, B*, 2002, **83**, 115–122.
6 M. E. Roberts, S. C. B. Mannsfeld, N. Queraltó, C. Reese, J. Locklin, W. Knoll and Z. Bao, *Proc. Natl. Acad. Sci. U. S. A.*, 2008, **105**, 12134–12139.
7 S. Casalini, F. Leonardi, T. Cramer and F. Biscarini, *Org. Electron.*, 2013, **14**, 156–163.
8 M. D. Angione, S. Cotrone, M. Magliulo, A. Mallardi, D. Altamura, C. Giannini, N. Cioffi, L. Sabbatini, E. Fratini, P. Baglioni, G. Scamarcio, G. Palazzo and L. Torsi, *Proc. Natl. Acad. Sci. U. S. A.*, 2012, **109**, 6429–6434.
9 M. Magliulo, A. Mallardi, M. Y. Mulla, S. Cotrone, B. R. Pistillo, P. Favia, I. Vikholm-Lundin, G. Palazzo and L. Torsi, *Adv. Mater.*, 2013, **25**, 2090–2094.

10 G. Scarpa, A.-L. Idzko, S. Götz and S. Thalhammer, *Macromol. Biosci.*, 2010, **10**, 378–383.
11 S. M. Goetz, C. M. Erlen, H. Grothe, B. Wolf, P. Lugli and G. Scarpa, *Org. Electron.*, 2009, **10**, 573–580.
12 L. Kergoat, L. Herlogsson, D. Braga, B. Piro, M.-C. Pham, X. Crispin, M. Berggren and G. Horowitz, *Adv. Mater.*, 2010, **22**, 2565–2569.
13 H. Klauk, *Chem. Soc. Rev.*, 2010, **39**, 2643–2666.
14 S. H. Kim, K. Hong, W. Xie, K. H. Lee, S. Zhang, T. P. Lodge and C. D. Frisbie, *Adv. Mater.*, 2013, **25**, 1822–1846.
15 S. H. Kim, K. Hong, W. Xie, K. H. Lee, S. Zhang, T. P. Lodge and C. D. Frisbie, *Adv. Mater.*, 2013, **25**, 1822–1846.
16 T. Cramer, A. Campana, F. Leonardi, S. Casalini, A. Kyndiah, M. Murgia and F. Biscarini, *J. Mater. Chem. B*, 2013, **1**, 3728–3741.
17 P. J. Boddy, *J. Electroanal. Chem.*, 1965, 199–244.
18 D. C. Grahame, *Chem. Rev.*, 1947, **41**, 441–501.
19 A. J. Bard and L. R. Faulkner, *Electrochemical Methods-Fundamentals and Applications*, Wiley, New York, 2001.
20 M. Waleed Shinwari, M. Jamal Deen and D. Landheer, *Microelectron. Reliab.*, 2007, **47**, 2025–2057.
21 M. E. Roberts, S. C. B. Mannsfeld, R. M. Stoltenberg and Z. Bao, *Org. Electron.*, 2009, **10**, 377–383.
22 C. J. Bettinger and Z. Bao, *Adv. Mater.*, 2010, **22**, 651–655.
23 T. Cramer, A. Kyndiah, M. Murgia, F. Leonardi, S. Casalini and F. Biscarini, *Appl. Phys. Lett.*, 2012, **100**, 143302.
24 M.-J. Spijkman, K. Myny, E. C. P. Smits, P. Heremans, P. W. M. Blom and D. M. de Leeuw, *Adv. Mater.*, 2011, **23**, 3231–3242.
25 A. Salleo, T. W. Chen, A. R. Völkel and R. A. Street, *Phys. Rev. B: Condens. Matter Mater. Phys.*, 2004, **70**, 1–10.
26 G. Tarabella, C. Santato, S. Y. Yang, S. Iannotta, G. G. Malliaras and F. Cicoira, *Appl. Phys. Lett.*, 2010, **97**, 123304.
27 G. Tarabella, C. Santato, S. Y. Yang, S. Iannotta, G. G. Malliaras and F. Cicoira, *Appl. Phys. Lett.*, 2010, **97**, 123304.
28 P. Lin, F. Yan and H. L. W. Chan, *ACS Appl. Mater. Interfaces*, 2010, **2**, 1637–1641.
29 A. Bolognesi, A. Di Carlo and P. Lugli, *Appl. Phys. Lett.*, 2002, **81**, 4646.
30 A. Bolognesi, M. Berliocchi, M. Manenti, A. Di Carlo, P. Lugli, K. Lmimouni and C. Dufour, *IEEE Trans. Electron Devices*, 2004, **51**, 1997–2003.
31 H. Helmholtz, *Ann. Phys. Chem.*, 1853, **165**, 211–233.
32 A. Khaliq, F. L. Xue and K. Varahramyan, *Microelectron. Eng.*, 2009, **86**, 2312–2315.
33 T. Cramer, T. Steinbrecher, T. Koslowski, D. A. Case, F. Biscarini and F. Zerbetto, *Phys. Rev. B: Condens. Matter Mater. Phys.*, 2009, **79**, 155316.
34 O. Stern, *Z. Elektrochem. Angew. Phys. Chem.*, 1924, **30**, 508–516.